Functional System Verification of the OPTEL-μ Laser Downlink System for Small Satellites in LEO

Thomas Dreischer, Björn Thieme, Klaus Buchheim
RUAG Schweiz AG, RUAG Space
Zurich, Switzerland
thomas.dreischer@ruag.com

***Abstract*—In 2010, RUAG Space has started with support from ESA the development of a complete system called OPTEL-μ for direct to ground laser downlinks from LEO satellites. It provides up to 2 Gbit/s information data rate and follows the request for the three elementary features small-ness, robustness and versatility. The emphasis lies on a compact and robust terminal that mainly addresses the needs of the emerging market of micro satellites to increase data download capabilities at comparable on-board resource constraints [1].**

Keywords—Optical downlink, Optel-μ, scintillation, micro vibration, direct detection, G-tilt, Rice, Beta distribution

I. INTRODUCTION

An engineering model (EM) of the OPTEL-μ space terminal and a proto-type of the optical ground terminal (OGT) have been developed under the project TESLA. Both have been subject to functional system verification which comprises a comprehensive analysis part and three main test campaigns that together form the TESLA system test. Established analytical models of the atmospheric channel were adapted and results from a mountain top test (MTT) campaign are described in [2]. Mission reports from LEO laser communications downlinks have additionally been considered, e.g. [7], [8], [9], [10]. Latter was especially of importance as far as pseudo wind speeds are concerned that are caused by fast angular motion of the slant path through the atmosphere during a LEO passage. The functional performance test structure thus comprises the MTT, an OGT PAT outdoor test and a laboratory indoor test campaign. The functional composition of a LEO-to-ground optical link was grouped such that three main functionalities can be tested:

1. Angular deviations at transmitter and receiver with respect to line-of-sight
2. Performance of the optical link with respect to fluctuating laser power due to platform pointing jitter and atmospheric turbulence
3. Achieved data rate and quality of service

This paper describes the tests performed and reports on the results. Conclusions are drawn on the end-to-end system performance and the space qualification planned in a follow on EQM development phase. An outlook will also be provided.

II. SYSTEM IN BRIEF

The OPTEL-μ system implements a bi-directional, asymmetric laser communications link from Low Earth Orbit to a fixed ground station as depicted below in Fig. 1.

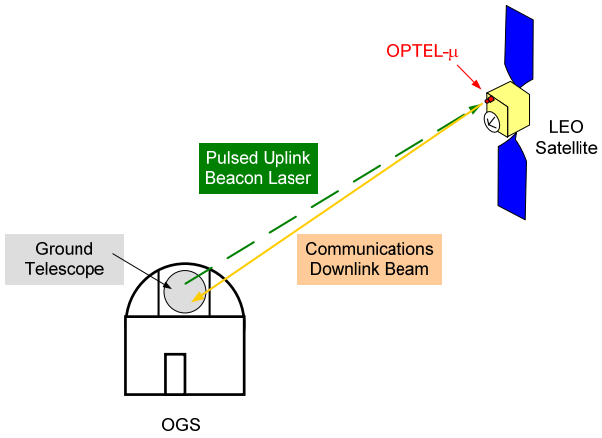

Fig. 1. Optical downlink scenario from LEO using the OPTEL μ system

The space system part comprises a miniature optical downlink terminal of ~5 kg mass and sub-45W DC power consumption. This allows for using the OPTEL-μ system on micro-satellites and on larger LEO platforms as an add-on to existing RF telemetry. To ease satellite integration, the space terminal is built in a modular way with 4 boxes as shown in Fig. 2, allowing for maximal flexibility w.r.t. accommodation.

Fig. 2. OPTEL-μ space terminal, 3 main units, rapid prototyping models (from left: Optical Head, Laser Unit, Electronics Unit)

Copyright (C) ICSOS2014. All Rights Reserved.

The baseline ground system consists of a global network of cost-efficient, eye-safe optical ground terminals (OGTs) that can be remotely controlled. For a commercially acceptable probability of 95% clear sky availability, an OGT network of seven optimal selected sites can achieve an aggregated data volume per day of about 6 Tbit (750 Gbyte) per space terminal.

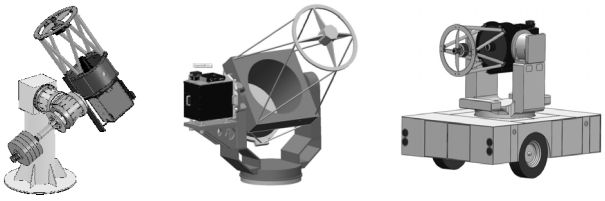

Fig. 3. OPTEL μ ground terminal, 3 elements (from left: ALT-ALT mount, ALT-AZ mount, Portable Unit)

Depending on the use case [1], the ground terminal for an OPTEL-μ space-to-ground link could be one of the 3 elements shown in Fig. 3. The ALT-ALT solution performs best in terms of motion because its singularity is at the local horizon. An ALT-AZ mount provides the inherent feature for sharing the same telescope with another instrument, for instance for space surveillance or satellite laser ranging. The optical tube assembly plus backend optics are designed to fit without change also on commercial, transportable high accuracy tracking mounts that carry 60 cm (24 inch) optical telescopes. A more detailed description of the different use cases and of the system's key parameters can be found in [1].

III. KEY PARAMETERS FOR SYSTEM TESTING

During the Engineering Model phase, the system level verification campaign concentrated on the physical layer, i.e., how to establish an optical link from a LEO satellite in space to a ground element. Analysis of overall network aspects and load cases will be carried on in parallel to the upcoming EQM development phase for the space hardware, aiming at TRL6.

The OPTEL-μ functional system verification comprises a comprehensive analysis part and three main test campaigns that together form the TESLA System Test. Mission reports from LEO downlinks have additionally been included to verify analytical models of the atmospheric channel.

Pointing analysis has been carried out to verify initial assumptions for both, space segment and various locations on ground. Visibility figures were computed over one mission elapsed year, taking into account ground elevation limits >15° w.r.t. local horizon, to cope with statistical variations of atmospheric distortions and to obtain high link availability under clear sky conditions. Also a ±10° sun exclusion angle was included.

Functional & performance testing comprises three devices under test, namely the space terminal, a representative ground terminal and a so-called "instrument box" that is attached to the telescope. It contains sensors and actuators required for fine alignment and communications receiver functionality. A tree of the functional performance test contributors to the LEO-Ground optical link verification is shown in Fig. 4

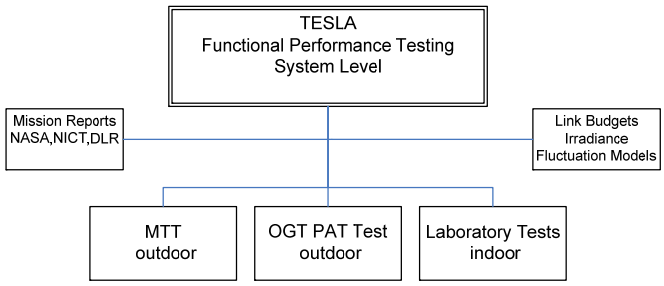

Fig. 4. Functional performance verification structure of the OPTEL μ system

Three main functionalities were tested

1. Angular deviations at transmitter and receiver with respect to line-of-sight
2. Performance robustness of the optical link with respect to fluctuating laser power caused by
   - Platform pointing jitter
   - Atmospheric turbulence
3. Achieved data rate and quality of service

In that context, the remainder of this section outlines various key parameters selected out of the vast parameter space for the OPTEL-μ system tests.

A. Atmospheric channel constraints

Intensity scintillation effects on the up- and downlink are caused by variations of the refractive index profile along the light path. This is modelled using the frozen turbulence hypothesis [11], a well-known approach that has been validated and reported in LEO-ground direct detection optical links like for instance by NASA, DLR-IKN, NICT, et.al. [8],[9],[10]. The OPTEL-μ system is designed for nominal operations at Fried parameters down to $r0_{1550nm} \geq 3$ cm. Spatial and temporal aperture averaging is applied at the direct detection ground receiver.

A static atmospheric channel test has been carried out over a slant range of 55 km. Even though limited to low elevation angles, hence strong boundary layer influences, key parameters could be verified that are related to multi-beam uplinks, comparison of scattering coefficients at different wavelengths and optical power scintillation statistics. The results of that so-called "mountain test campaign" (MTT) are reported in [2].

Taking into account the MTT results, the downlink scintillation index has been modelled for 1550 nm at different site altitudes, based on plane wave formula from [11]. Plausibility checks are in line with test data reported from 800 nm LEO downlinks [8], [9], [10].

Fig. 5 shows expected scintillation characteristics during daytime. The upper set of curves depicts the Rytov variance of a point receiver, and the lower set of curves shows the reduction effect of aperture averaging, taking into account the 60 cm OGT prototype. Worst case values of around SI=0.1 have to be expected at ground elevation angles <20° at 400 m altitude above sea level. This is taken as design parameter.

Copyright (C) ICSOS2014. All Rights Reserved.

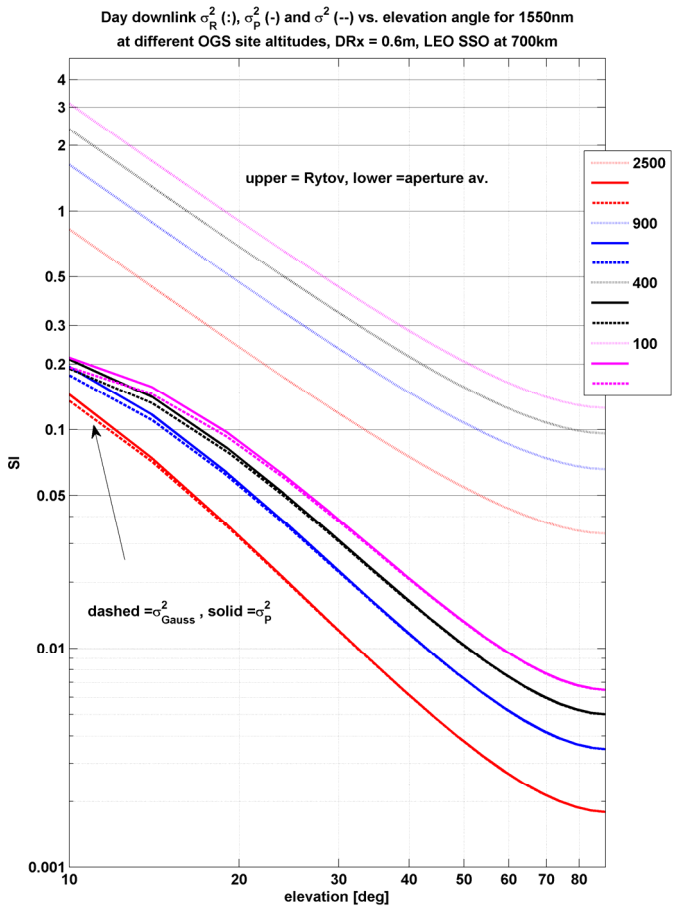

Fig. 5. Scaled temporal power spectrum of an incident plane wave versus radial frequency

Uplink scintillations were modelled using a spherical wave approach [11][12]. The ground uplink furthermore applies four incoherent beams that lead to a considerable reduction of the uplink scintillation index. MTT results showed that careful co-alignment is a key to obtain reduction of uplink scintillation.

LEO motion w.r.t. ground causes much faster temporal irradiance spectra like those known from stellar observations or from ground-to-GEO laser communications. The motion of line of sight through the atmosphere on a deg/s time scale causes high pseudo wind speeds especially in high altitudes. Such characteristics take influence on the temporal spectra of irradiance fluctuations and they influence temporal spectra of tip/tilt center of gravity tracking. The way of modelling those characteristics is well understood and established models were already validated and reported in LEO-ground missions [7].

The LEO-ground link comprises large angle motion of the ground terminal when a LEO passage is acquired and tracked. This motion is tested in outdoor configuration in a so-called "OGT PAT Test". The OGT PAT Test uses a prototype OPTEL-μ ground receiver terminal with a 60 cm telescope. As tip/tilt angle of arrival in a LEO-ground link is independent from wavelength [5], it is possible to conduct the OGT PAT Test using visible light reflected from a LEO satellite. The combination between the large angle motion outdoor pointing test and the small angular motion in the laboratory test bed is simply achieved by recording residual angle of arrival fluctuations in outdoor configuration and "play back" in laboratory environment, scaled to the optical laboratory setup that is without telescope, hence requires appropriate magnification of the tip/tilt angles recorded "in the sky". Anticipated characteristics have already been calculated in a parametric analysis, using G-tilt spectra and taking into account the potential impact of wind gusts [6]. From [5], the G-tilt can be modelled as

$$\Phi_g(f) = 0.31 \cdot D^{-1/3} \sec(\zeta)\, f^{-3/8} \int_{h0}^{H} C_n^2(h) \cdot \left(\frac{v}{D_{Rx}}\right)^{5/3} dh \cdot F_G(f/v) \quad (1)$$

with

$$F_G(y) = \int_0^1 \frac{x^{5/3}}{\sqrt{(1-x^2)}} J_1^2(\pi \cdot y/x)$$

A resulting spectra for 700 km SSO, 400 m site altitude, as shown below in Fig. 6.

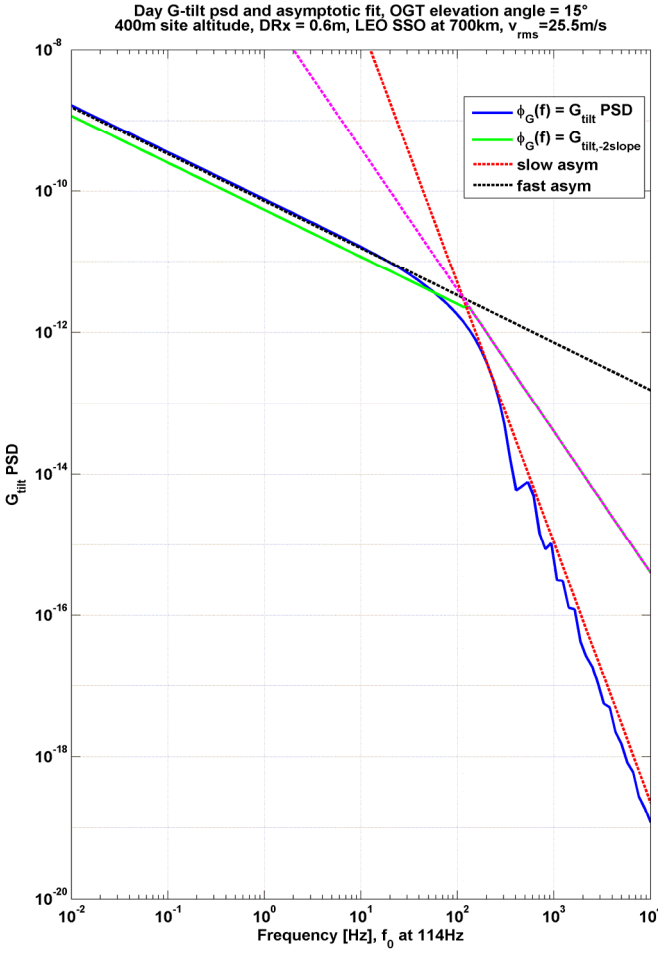

Fig. 6. Daytime G-tilt spectra for 700km LEO SSO, OGS 400m a.s.l, high zenith angle, used to dimension the angle-of-arrival tracking control loop

The anticipated temporal spectra were modelled based on [11]. This approach can directly be compared to measurements reported from a LEO downlink in [7], taking additionally into account the different wavelengths and receiver apertures used.

Copyright (C) ICSOS2014. All Rights Reserved.

The modelled temporal effect is the shift of power concentration that gets reversed from the point aperture case, levelling greatest power concentrations toward the lower frequencies once finite aperture diameter receivers are introduced, as described in [11]. The effect is described by integrating the temporal covariance function $BI(\tau,D_{Rx})$ as shown below in equation (2).

$$S_I(\omega, D_{Rx}) = \frac{4}{\omega_t}\int_0^{\infty} B_I\left(\frac{s}{\omega_t}, D_{Rx}\right)\cdot\cos\left(\frac{\omega\cdot s}{\omega_t}\right)ds \qquad (2)$$

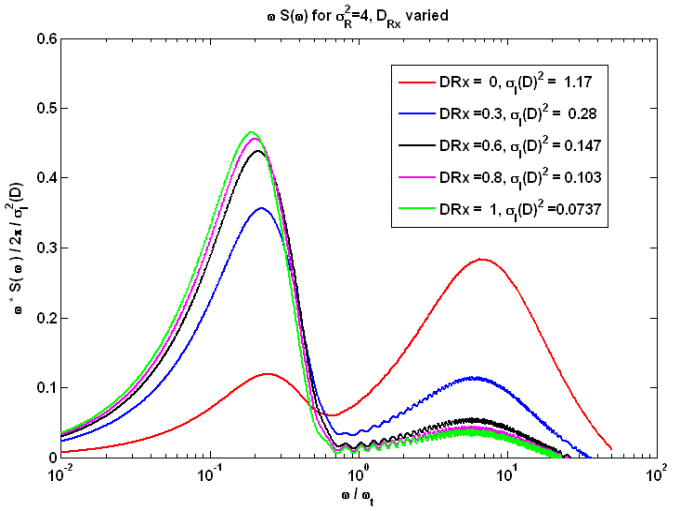

Fig. 7. Scaled temporal power spectrum of an incident plane wave versus radial frequency

Fig. 7 shows an example for the temporal co-variance function for a plane wave case of strong turbulence (example: $(\sigma^2_R=4)$. A significant power re-distribution from ω_t toward $0.2\omega_t$ is observed, with a high frequency portion at $\sim 5\omega_t$ for point apertures. However, only a moderate re-distribution of power from ω_t toward $0.5\omega_t$ should be expected as long as $\sigma_R^2<1$.

B. *Overall fade probabilities*

In general, the OPTEL-μ laser communications downlink aims at a balanced design with respect to intensity fluctuations. In other words, intensity fluctuations at the communications ground receiver that are caused by space terminal mispointing (jitter) shall be similar or comparable to those caused by (weak) lognormal distributed atmospheric turbulence. At a given zenith angle, 95% or higher of all received power drops at the OGT receiver shall remain less than the allocated overall scintillation margin for that zenith angle.

C. *System Test Parameters*

The functional system test focusses at daytime downlink conditions from a near-polar, 700 km reference orbit and a ground terminal located 400 m above sea level. A list of key parameters used during system testing is shown in TABLE I.

TABLE I. ATMOSPHERIC KEY PARAMETERS FOR FUNCTIONAL PERFORMANCE TESTING OF OPTEL-μ SYSTEM

Link direction	**LEO-ground test parameters**		
	Key parameter	***Value***	***Unit***
4-beam uplink, untracked	$\sigma^2_{I\_up,total\ ,\ 1064nm}$ $(\sigma_R=1.5)$	0.66	-
	$v_{\perp,20°}$	73	m/s
	$v_{\perp,zenith}$	142	m/s
	$f_{t,20°}$	192	Hz
	$f_{t,zenith°}$	644	Hz
4-beam uplink, tracked	$\sigma^2_{I\_up,total,\ 1064nm}$ $(\sigma_R=1.5)$	0.45	-
	$v_{\perp,20°}$	73	m/s
	$v_{\perp,zenith}$	142	m/s
	$f_{t,20°}$	192	Hz
	$f_{t,zenith°}$	644	Hz
Downlink beam	$\sigma^2_{P\_dwn,\ 1550nm}$ $(\sigma_R=0.5)$	0.1	-
	$v_{\perp,20°}$	73	m/s
	$v_{\perp,zenith°}$	142	m/s
	$f_{t,20°}$	192	Hz
	$f_{t,zenith°}$	644	Hz
min. site altitude	above sea level	400	m
min. zenith angle		75	deg
orbital altitude	(→angular speeds)	400..900	km

D. *Microvibration pointing jitter*

Platform jitter and attitude drift, in space and on ground are relevant parameters for functional performance testing on system level. For the ground terminal, platform attitude performance and jitter are specified based on manufacturer's heritage and take into account practical experience from satellite laser ranging and debris tracking stations. In space segment, data reported from micro-satellite operators is used.

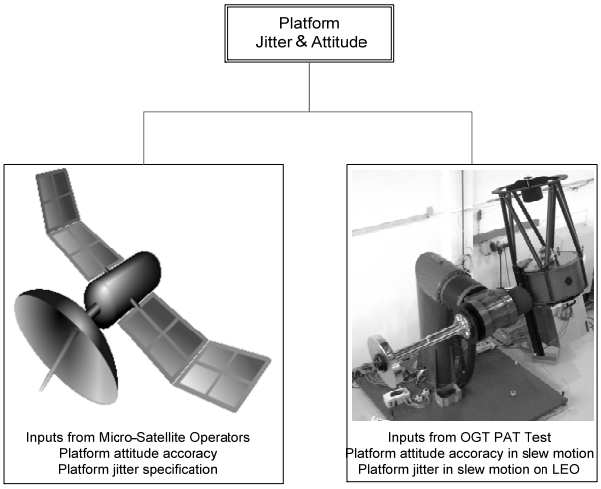

Fig. 8. Inputs for platform attitude and –jitter for laboratory form part of system test key parameters

Copyright (C) ICSOS2014. All Rights Reserved.

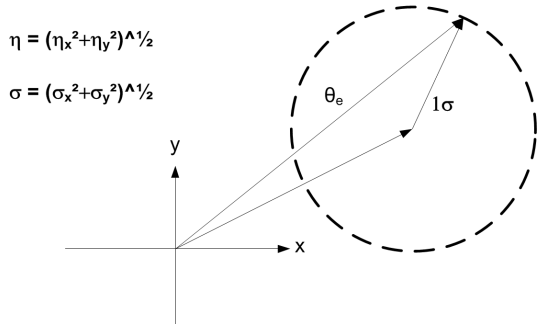

Fig. 9. Vector diagram for composition of radial pointing error

The theory for deduction of a radial pointing jitter from two independent orthogonal axial jitter components $\{\theta_x, \eta_x, \theta_y, \eta_y\}$ is well known and described in [14]. The model uses two independent random variables θ_x, θ_y, with mean values η_x,η_y and variance σ^2_x, σ^2_y.

For mechanical induced vibration jitter, it often suffices to let $\sigma^2_x = \sigma^2_y = \sigma^2$. The resulting Rice probability density distribution is shown in equation (3).

$$p(\theta_e) = \frac{\theta_e}{\sigma^2}\exp\left[-\frac{1}{2\sigma^2}\left(\theta_e^2+\eta^2\right)\right]\cdot I_0\left(\frac{\theta_e\eta}{\sigma^2}\right)$$
$$\text{with} \qquad (3)$$
$$\theta_e(t) = \left(\theta_x(t)^2+\theta_y(t)^2\right)^{1/2},\ \eta = \left(\eta_x^{\,2}+\eta_y^{\,2}\right)^{1/2}$$

Fig. 10 shows a typical statistical distribution of micro vibration jitter for angles related to the 1/e2 divergence half angle. Confidence intervals were set to 5%.

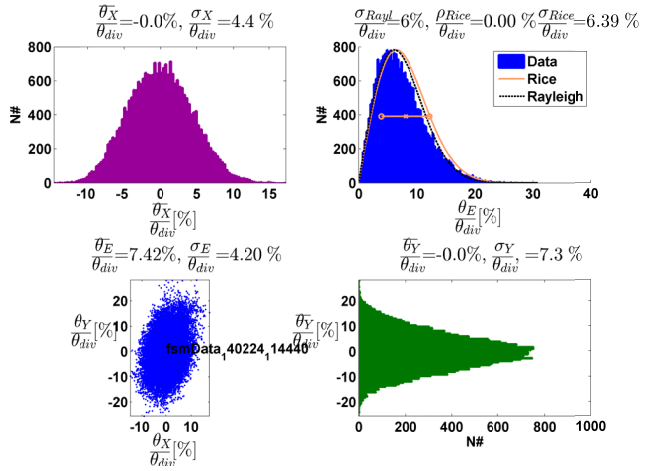

Fig. 10. Measured statistical distribution of axial and radial tracking errors during standstill, microvibration activated

It is η=0 in that measurement, hence the Rice distribution reduces to the well-known Ryleigh distribution. A cross-check between observed variance and observed mean with the same quantities determined from the fitted Rayleigh model shows the validity boundaries of that fit approach.

TABLE II. COMPARISON OF OBSERVED MEAN AND VARIANCE

Mean, Variance from σ_{Rayl}=6.03%		
Table column subhead	***Calculated***	***observed***
$\text{mean} = \sqrt{\pi/2}\cdot\sigma_{Rayleigh}$	7.5%	7.4%
$\text{variance} = (4-\pi)/2\cdot\sigma^2_{\text{Rayleigh}}$	15.6%	17.6%

The Rice distribution in equation (3) is used for analyzing a space terminal's radial pointing characteristics including bias. The OPTEL-μ space pointing system tolerates a bias error contribution that can reach magnitudes up to the jitter, hence can become non-negligible.

The transmitter optical gain as a function of the radial mispointing error θ_E is modelled from [13] for a central obscured aperture with obscuration ratio γ as follows:

$$G_{Tx}(\theta_e;\alpha,\beta,\gamma) = \left(\frac{\pi\cdot D_{Tx}}{\lambda}\right)^2\cdot g_T(\theta_e;\alpha,\beta,\gamma) \qquad (4)$$

and for $g_T(\theta_e;\alpha,\beta,\gamma)$ with $a = D_{Tx}/2,\ \gamma = b/a$

$$g_T(\theta_e;\alpha,\beta,\gamma) = 2\alpha^2\cdot\int_{\gamma^2}^{1}\exp(j\beta u)\cdot e^{(-\alpha^2 u)}\cdot J_0\left[ka\sin(\theta)\sqrt{u}\right]du \qquad (5)$$

The term β includes near-field and defocusing effects and it has significant impact on both, the antenna gain and the off-pointing gain characteristics, also under far field condition. β is defined for a link distance z for R as waveform radius of curvature before refraction and it yields

$$\beta = \frac{2\pi}{\lambda}\cdot a^2\cdot\left[\frac{1}{z}+\frac{1}{R}\right] \qquad (6)$$

As a consequence of the presence of potential bias pointing errors, the known modelling approach from [4] that combines motion jitter loss with atmospheric intensity fluctuations has been slightly modified. The more general form of the beta distribution is used to account for an additional bias error impact in the beta-distributed transmit power fluctuations. The transmit power distribution, normalized to 0 dB, then becomes

$$p_{\text{TxGain}}(x;a,b) = \frac{1}{B(a,b)}\cdot x^{(a-1)}\cdot(1-x)^{b-1} \qquad (7)$$

Using the Gamma function representation of B(a,b), the extended beta distribution can be reduced for no bias errors, hence b=1, to

$$B(a,b=1) = \frac{\Gamma(a)\cdot\Gamma(1)}{\Gamma(a+1)} = \frac{\Gamma(a)}{\Gamma(a+1)} = \frac{\Gamma(a)}{a\cdot\Gamma(a)} = \frac{1}{a} \qquad (8)$$

which for equation (7) leads to the well-known compact form for beta distributed transmit power

$$p_{\text{TxGain}}(x;a,1) = a\cdot x^{(a-1)} \qquad (9)$$

Copyright (C) ICSOS2014. All Rights Reserved.

IV. Ground Terminal Outdoor Tracking Test

The OGT PAT Test uses a representative optical ground terminal (OGT) in ALT-ALT configuration with a 60 cm optical tube assembly and a lasercom instrument box attached to the Cassegrain focus, like shown in Fig. 11 at its test site. In the following, the OGT is referred as *Device Under Test 3* (DUT3).

Fig. 11. 60 cm Ground Terminal (DUT3) during satellite tracking testing

A visible tracking system was equipped to DUT3 and outdoor tests comprise the acquisition and tracking of near-polar LEO satellites illuminated by the Sun. Open loop pointing characteristics of DUT3 were measured at various zenith angle ranges with temporal resolution of tracking camera output at several 10 s and 100 s of Hertz readout rates. High speed camera recordings from closed loop tracking configuration were stored for later play-back in laboratory environment, allowing for verification of the fine steering loop performance. The fine tracking performance of the OGT has then been characterized under condition of large angle motion effects and it fulfills well the specified accuracies as shown in Fig. 12.

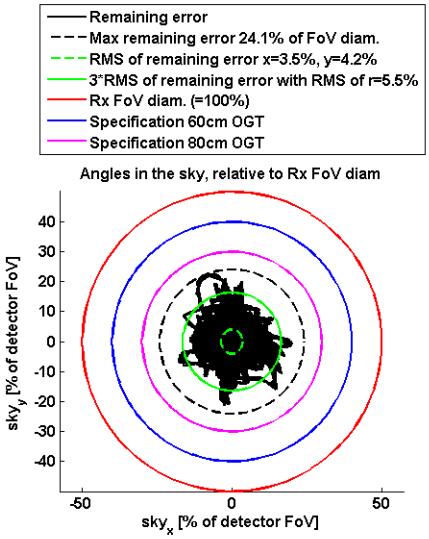

Fig. 12. Measured ground tracking error related to Rx detector field-of-view

V. System Testing in Laboratory

The system test bed allows for testing of the bi-directional laser communications link during presence of angular motion and fluctuating optical signal levels.

A. System Test Setup

Two devices under test are located in close proximity to a large optical table that is decoupled from base motion jitter of the building. A vibrating gimbal simulates satellite motion and jitter in laboratory environment. Angle-of-Arrival (AoA) motion and residual coarse tracking errors at the ground terminal are introduced by a fast "AoA" tip/tilt mirror.

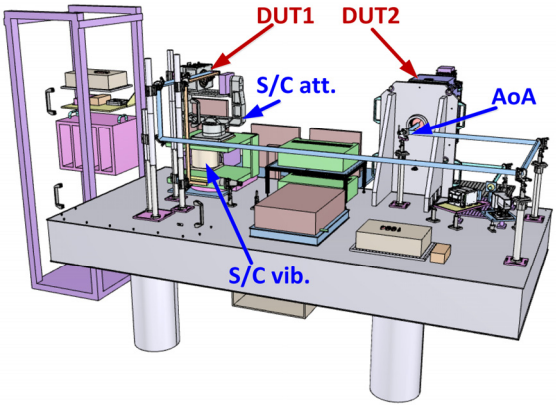

Fig. 13. Laboratory test setup for functional performance testing (Space Terminal =DUT1, Ground Terminal instrument box =DUT2)

The space terminal functionality is distributed over four physical boxes that are shown in Fig. 14. As an exception, the electronics unit was built at a larger volume for cost reasons. Parts placement for a tighter realization has been established in parallel and updated after consolidation of fundamental design choices after completion of the functional system tests.

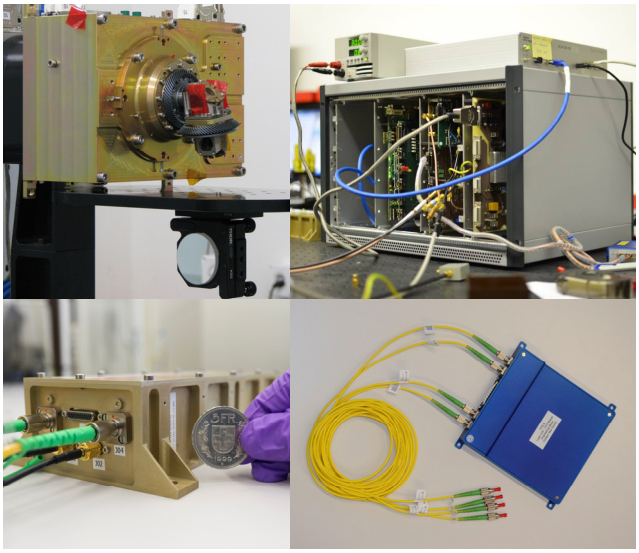

Fig. 14. The Space Terminal (DUT1) consists of 4 boxes (clockwise from upper left: Optical Head Unit, Electronics Unit, Optical Fiber Amplifier, Pulse Laser Transmitter)

Copyright (C) ICSOS2014. All Rights Reserved.

B. *Pointing, Acquisition, Tracking Testing*

Two different ways for spatial acquisition are implemented. The optical ground terminal scans for the satellite and the space terminal re-directs its communications beam or its space beacon beam once getting illuminated. Or the space terminal scans its beacon over the uncertainty cone until the ground terminal receives an optical signal. The ground terminal can then re-direct its own beacon more accurately towards the Space Terminal and illuminate it permanently. As soon as the space terminal detects the ground beacon it stops scanning, points in the direction of the received uplink beacon that is sent from ground and finally tracks the ground beacon signal.

During the PAT tests of the Optel-μ the scanning of the Space Terminal, the pointing in the direction of the Ground Terminal and the transition into Tracking has been tested for different angular velocities that include orbital motion in altitudes between 700 km and 400 km plus superimposed motion that stems from potential attitude maneuvers.

The acquisition process is the same at ground terminal and at space terminal. Fig. 15 and Fig. 16 show test results from spatial acquisition sequences, seen at space terminal level.

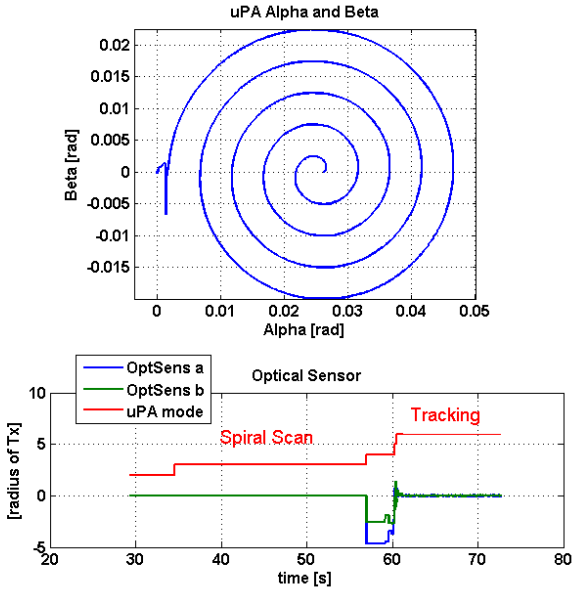

Fig. 15. Angular motion in spatial acquisition (Test_05-Mar-2014_cntrl05)

The upper part of each figure shows the search motion in x/y view. In Fig. 15 the space terminal is at stand still for plausibility check, in Fig. 16 the space terminal acquires out of a superimposed angular motion in negative alpha direction.

The lower part of each plots show the operational modes and the data of the relevant sensor, which are

- the Acquisition Sensor (AS) during Scanning, Stopping and a short tracking period on the AS and
- the Tracking Sensor during the final tracking phase

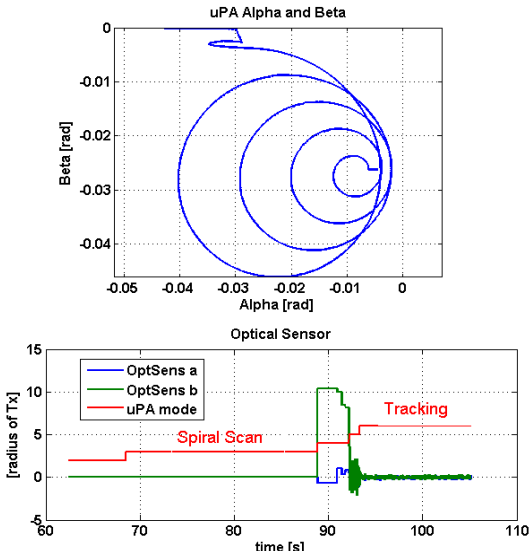

Fig. 16. Angular motion in spatial acquisition (Test_05-Mar-2014_cntrl06)

A zero of the Acquisition Sensor during the Spiral Scan motion means that there is no valid AS data, either because there is no detected spot available or temporarily due to scintillation of the uplink beacon signal. During the stopping and back positioning to the initially detected spot position there is no new AS data read out. In this phase the Space Terminal acts autonomous and relies on regular updates on current S/C pointing and attitude information. Hence it is not necessary that it is permanently illuminated by the Ground Terminal even though this is nominally the case.

C. *Pointing during Tracking*

Once acquired, of interest is how accurate the spatial tracking can be maintained under presence of platform vibrations and fluctuating optical signal levels. Fig. 17 shows the open loop pointing error of the ground terminal. Apart from drift, deviations remain ≤ 1 arcsec. Once acquired, without further optimization, the OGT can point at the satellite in open loop and keep it within the tracking field of view during several minutes, for instance during partial cloudy sky. Sound tracking margin is available for both, 60 cm and 80 cm telescope implementation without the need for adapting the laser communications instrument box per telescope diameter.

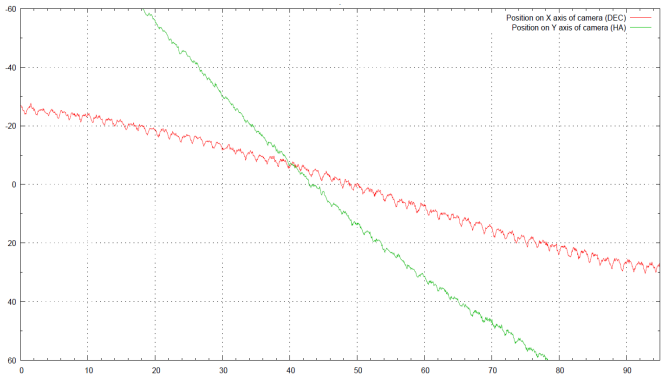

Fig. 17. Open loop tracking error (arcsec) versus time (sec), DUT3 test

Copyright (C) ICSOS2014. All Rights Reserved.

The ground terminal's uplink beacon divergence has been designed with sound margin, hence no dedicated pointing test was required. It is valid to take into account the residual tracking error and add a minor bias contribution that stems from residual errors during self-alignment calibration between receive and transmit beam directions.

A profound characterization of Tracking and Pointing performance at Space Terminal level has been carried out for different angular velocities that include the satellite's orbital motion in altitudes between 700 km and 400 km plus superimposed angular motion from potential attitude maneuvers. Fig. 18 shows the statistical distribution of measured residual tracking errors related to Tx divergence angle for a 700 km sun-synchronous orbit (SSO), with motion profile selected at low ground elevation angle and lowest receive power level. Confidence intervals were set to 5%.

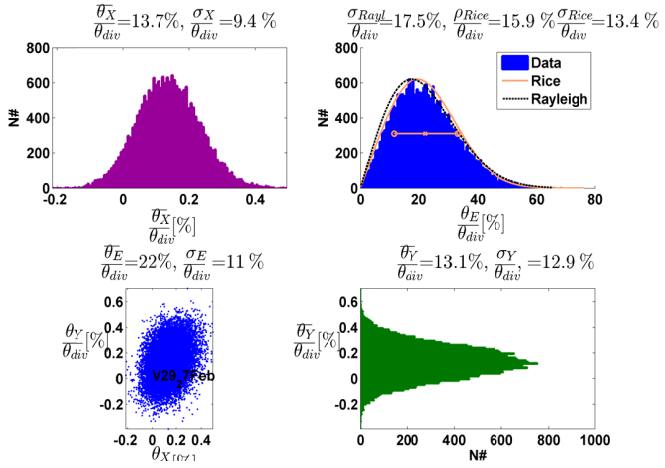

Fig. 18. Measured statistical distribution of residual tracking errors related to Tx divergence angle, 700km sun-synchronous orbit

Fig. 19 summarizes the resulting pointing error statistics for four different measurements at a 700 km SSO example. Tracking power and ground elevation angles were varied, resulting in different angular speed and different scintillation.

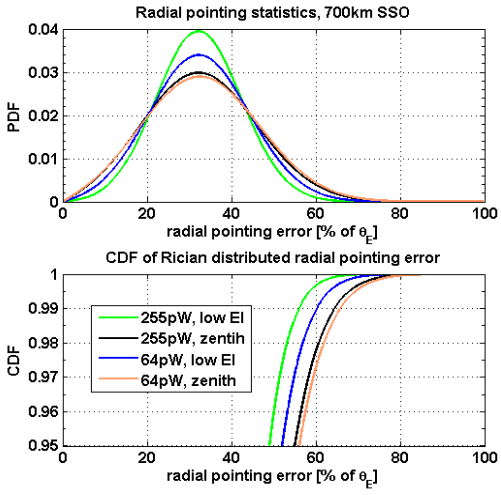

Fig. 19. Pointing error statistics related to Tx divergence angle, average tracking power levels varied over 6 dB, near zenith and low elevation scenario

Using equation (4), (5) and (7) allows for calculating statistical fluctuations of transmit power levels, pending the full characterization of the transmit antenna far field gain pattern.

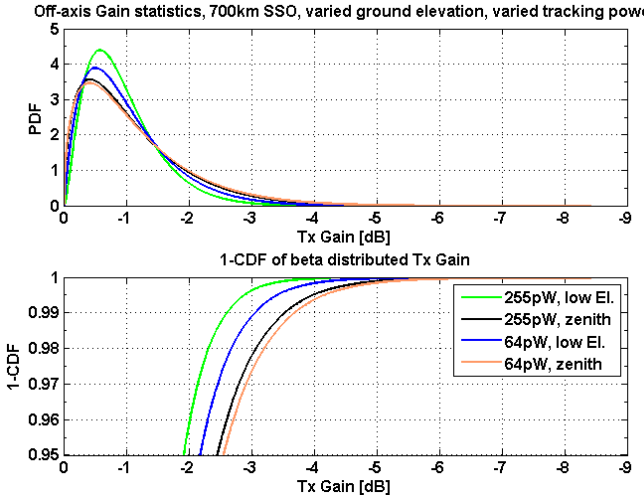

Fig. 20. Transmit gain statistics at space terminal due to radial pointing error

When taking into account the findings from OHU pointing measurements, the bias errors cannot be considered negligible, hence the model has to be updated to include that bias pointing effect. The resulting total normalized intensity can be expressed using the weak turbulence pdf and combine this with the extended beta distribution pdf for bias errors, like shown in equation (10)

$$p_{PRx,OGT}(i_t) = \int_0^1 p_{TxGain}(x;a,b) \cdot p_{turb}\left(\frac{i_t}{x}\right)\frac{dx}{x}. \qquad (10)$$

Using equation (7) for p_{TxGain} and assuming lognormal intensity distribution p_{turb}, the total intensity pdf gets

$$p_{PRx,OGT}(i_t) = \int_0^1 \frac{\Gamma(a+b)}{\Gamma(a)\cdot\Gamma(b)} \cdot \frac{x^{(a-1)}\cdot(1-x)^{b-1}}{\sqrt{2\pi\sigma_I^{\,2}}\cdot i_t/x} \cdot \exp\left\{-\frac{\left[\ln\left(\frac{i_t}{x}\right)+\frac{\sigma_I^{\,2}}{2}\right]^2}{2\sigma_I^{\,2}}\right\}\frac{dx}{x} \qquad (11)$$

The resulting scintillation statistics are depicted in Fig. 21.

Numerical analysis was carried out, using the CDF derived from $p_{Rx,OGT}$. Synthesized scintillation data at ground receiver were generated using uniform random numbers with the inverse CDF from $p_{Rx,OGT}$ and applying the spectral envelope from equation (2). Fig. 21 shows cumulative probability statistics for the worst case scenario with largest transmit pointing errors at the space terminal and highest atmospheric scintillation index at the ground terminal. When compared to the ideal case of no bias pointing error, the presence of worst case bias pointing errors (lower curves) amounts requires an additional allocation of ~+1 dB scintillation margin.

These worst case scintillation characteristics incl. bias pointing errors were measured at the communications subsystem to be in line with the allocated corresponding scintillation margin, hence, confirm a balanced overall design.

Copyright (C) ICSOS2014. All Rights Reserved.

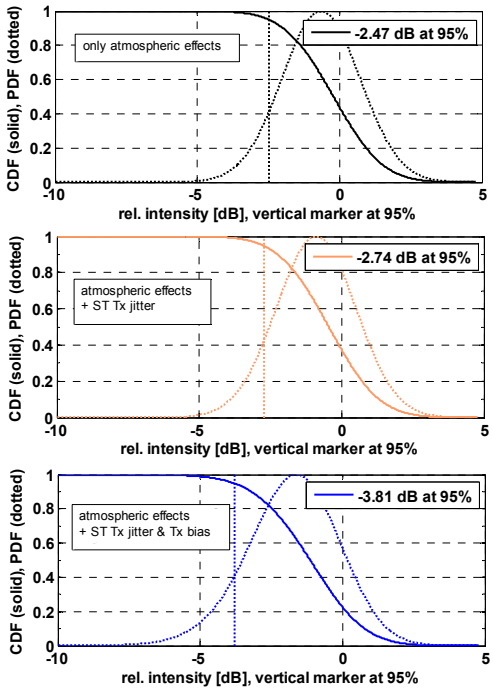

Fig. 21. Impact of worst case Tx bias error on scintillation margin at ground receiver, SI=0.1

D. Communications Testing

Along-track optimization of data rate during a passage was tested using automated repeat request via an optical uplink channel that is modulated onto the uplink beacon laser. Data rate is optimally adjusted, taking into account variation of zenith angle, hence varying link distance, power scintillation margin and optional additional sub-visible cirrus cloud attenuation. These effects are being tested in the system test bed for key parameters listed in TABLE I.

An example for OOK modulation testing is depicted below in Fig. 22. Measured sensitivities with and without automated repeat request (ARQ) are shown both, under presence of intensity scintillations and without scintillation for comparison.

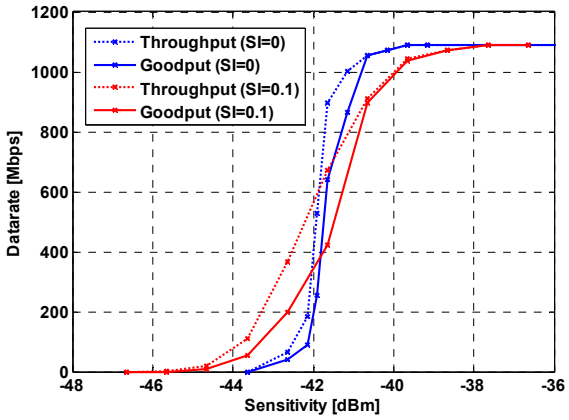

Fig. 22. Measured receiver sensitivities, with and without fluctuating receive power signals (atmospheric turbulence & space terminal pointing jitter)

Convolutional coding with code rate 7/8 was applied. Additional tests are being carried out for PPM format, aiming at higher data goodput at long link distances. The measured sensitivities are in line with the overall link budget allocations.

VI. System Test Summary

An engineering model (EM) of the OPTEL-μ space terminal (ST) and a proto-type of the optical ground terminal (OGT) have been developed. Both, ST and OGT have been subject to extensive functional system verification. The activity has been split into a comprehensive analysis part and three test campaigns that together form the TESLA system test. Key parameters for system testing have been reported and corresponding analytical formula have been shown. Tests have been described and results been have discussed.

A. Conclusions & Outlook

The test results confirm sound margins for line-of-sight steering and tracking control on ground terminal side. The space terminal's (ST) acquisition and tracking subsystem shows robustness against satellite vibrations and potential attitude maneuvers, including margin for bias pointing errors. The ST fulfils its pointing accuracy requirements at 99% probability instead of specified 95% which leaves some design margin for the next development phase.

The communications subsystem meets the specified receiver sensitivity described in sub section V.D. It has proven to be robust against interruption (e.g. partial cloud blockage during a downlink). Furthermore it is also highly flexible in adaptation to variations of channel attenuation by adjusting its code rate or by adaptation of the modulation format.

The project is now ready for entering the EQM design, qualification and test phase in the following months, aiming at TRL6. On software side, this includes the implementation of comprehensive automated mode switching and automated along-track optimization of data rate during a passage.

Discussions with several spacecraft operators are on-going to prepare for an In Orbit Demonstration activity around 2016.

Acknowledgment

This project was made under ESA contract number 4000104805/11/NL/US. We express our gratitude to Mr. P. van Loock, Dr. Z. Sodnik and Mr. D. Schmitt at ESA, and to Dr. P. Guggenbach and Dr. H. Wentscher RUAG Schweiz AG for their continued support in the execution of this work.

References

[1] T. Dreischer, K. Buchheim, B. Thieme, L. Pryce, "AN OPTICAL PAYLOAD DATA TRANSMISSION SYSTEM FOR SMALL SATELLITES IN LEO", TTC 2013, 6th ESA International Workshop on Tracking, Telemetry and Command Systems for Space Applications, ESA-ESOC, 10 - 13 September 2013

[2] M. Mosberger, T. Dreischer, M. Bacher, "Mountain-top-to-valley optical link demonstration as part of a miniature terminal development," Photonics West 2013, SPIE 8610-6

Copyright (C) ICSOS2014. All Rights Reserved.

[3] T. Dreischer, S. Herold, T. Jungblut, Active Regulated System for Long Haul Free Space Laser Communications, Adaptronics Congress, Darmstadt, Germany, 2011

[4] K. Kiasaleh, "On the probability density function of signal intensity in free-space optical communications systems by pointing jitter and turbulence", Opt.Eng., 1994, Vol. 33, No. 11

[5] A. Tyler, "Bandwidth considerations for tracking through strong turbulence", OSA Journal Volume 11, Issue 1, 1992, pp. 358-367.

[6] E.J. Kibblewhite, M.R. Chun, "Design of tip tilt and adaptive optics servos using measured angle-of-arrival and phase power spectra", SPIE Vol. 3353, 1998

[7] M. Toyoshima et al, "Frequency characteristics of atmospheric turbulence in space-to-ground laser links", SPIE Vol. 7685, 2010

[8] M. Toyoshima et al, Data analysis results from the KODEN experiments, SPIE Vol. 6709, 2007

[9] N. Perlot, "Results of the Optical Downlink Experiment KIODO from OICETS", SPIE Vol. 6457, 2007

[10] J. Kovalik at al, "Data products from OCTL to OICETS Optical Link experiment", SPIE Vol. 7587, 2010

[11] L.C. Andrews, R.L. Phillips, "Laser Beam Propagation through Random Media", SPIE Press, second edition 2005

[12] S. F. Clifford, "Temporal-Frequency Spectra for a Spherical Wave Propagating through Atmospheric Turbulence", OSA Vol. 61, 1971

[13] Klein, Degnan, "Optical Antenna Gain, 1: Transmitting Antennas", Appl. Opt. 13,9, Sept. 1974

[14] Vilnrotter, "The effects of Pointing Errors on the Performance of Optical Communications Systems", IPN Progress Report 1981

Copyright (C) ICSOS2014. All Rights Reserved.